Exploiting Rapidly Time-Varying Sparsity for Underwater Acoustic Communication

Weihua Jiang, *Member, IEEE*, Feng Tong, *Member, IEEE*, and Zhengliang Zhu

***Abstract*—Due to the combined effects of different acoustic propagation, reflection patterns in different time-scale, time-varying underwater acoustic (UWA) channel generally exhibits hybrid sparsity, i.e., contains not only rapidly time-varying elements, but also stationary or slowly time-varying ones. While the classic sparse reconstruction algorithms such as orthogonal matching pursuit (OMP) generally do not take it into account, the existence of static multipath will unavoidably hinder the tracking of rapid time variations. In this paper, a sequential adaptive observation length orthogonal matching pursuit (SAOLOMP) approach is proposed to sequentially explore rapidly time-varying sparsity in a two-step sequential manner. Specifically, the static components are firstly separated via simultaneous orthogonal matching pursuit (SOMP) among continuous measurements. Upon the residual error of the SOMP, the measurement-wise OMP is applied for estimating the remained dynamic components. As the variation of the SOMP residual error indicates how rapidly the remained dynamic multipath components vary, the observation length of the OMP is adjusted according to the gradient of residual error to adapt to rapidly time-varying components. Finally, both types of sparse components are summed up to obtain the whole channel response. Numerical simulations as well as experimental results from field UWA communication data show that the proposed algorithm exhibits better performance in exploiting rapidly time-varying sparsity than the state-of-the-art compressive methods do under UWA channel.**

***Index Terms*—Hybrid sparse, rapidly time-varying, sequential adaptive observation length orthogonal matching pursuit, underwater acoustic communication.**

I. Introduction

With the increasing demand of marine information acquisition and transmission, underwater acoustic (UWA) communication technology has drawn more and more attention in diverse marine fields [1]–[3]. However, UWA channel is recognized as an extremely adverse wireless channel with time-space-frequency variation, strong multipath, limited bandwidth and high noise [4]–[6], rendering UWA communication a highly challenging mission. One of the typical difficulties is that, the complicated characteristics of UWA channel pose significant limitation on the estimation and equalization of UWA channel for improving the UWA communication performance.

Under the framework of compressed sensing, the sparse characteristic of UWA channel can be explored to improve the communication performance and reduce the noise interference [7], [8]. While the research community is trying to find the sparse solution by minimizing the l_0 norm, directly searching for the minimum l_0 norm will inevitably cause NP hard problem [9]–[11]. Besides, it is easily affected by noise, because any slight noise will be possibly identified as the nonzero elements. Plenty of approximation algorithms are studied to solve the problems introduced by l_0 norm [9]–[12], such as the smoothing l_0-norm (SL0) [12].

The greedy algorithm has been commonly used to recover sparse signals, which includes methods such as matching pursuit (MP) [13] and orthogonal matching pursuit (OMP) [14]. Due to its noise robustness in sparse recovery, greedy method gains extensive applications for the estimation of sparse UWA channel. Within several continuous measurement windows, the static sparse channel generates substantial correlations [15], [16], which has been applied for improving the UWA channel estimation performance under the framework of joint sparse recovery [17], [18]. Note that, a popularly known variant of the OMP algorithm for joint sparse recovery is simultaneous OMP (SOMP) [15]. Nevertheless, most of the compressed sensing algorithms do not take care of the time-varying characteristics of UWA channel.

On the other side, for the UWA channel with dynamic sparsity, based on the dynamic compressed sensing theory [19]–[23], Kalman Filtered Compressed Sensing (KF-CS) has been investigated to the recovery of time-varying sparsity by combining a reduced order Kalman filter (KF) with CS. However, for UWA channel, with the exception of rapidly time-varying paths such as those caused by dynamic sea surface, there also exist static or slowly time-varying paths, including those experiencing direct propagation or bottom reflection. In other words, UWA channel generally contains hybrid sparsity [24]. Since the rapidly time-varying multipath is usually generated by highly dynamic sea surface, typical UWA channels may simultaneously exist both static components and rapidly time-varying ones, such as

Manuscript received 25 August 2021; revised 29 November 2021, 8 March 2022, and 21 April 2022; accepted 6 June 2022. Date of publication 13 June 2022; date of current version 19 September 2022. This work was supported in part by the National Key Research and Development Program of China under Grant 2018YFE0110000 and in part by the National Natural Science Foundation of China under Grants 11274259 and 11574258. The review of this article was coordinated by Prof. Byonghyo Shim. *(Corresponding author: Feng Tong.)*

Weihua Jiang is with the Key Laboratory of Underwater Acoustic Communication and Marine Information Technology of the Ministry of Education, Xiamen, Fujian 361005, China, with the College of Ocean and Earth Sciences, Xiamen University, Xiamen, Fujian 361005, China, and also with the Department of Marine Technologies, University of Haifa, Haifa 3498838, Israel (e-mail: hwjiang@stu.xmu.edu.cn).

Feng Tong and Zhengliang Zhu are with the Key Laboratory of Underwater Acoustic Communication and Marine Information Technology of the Ministry of Education, Xiamen, Fujian 361005, China, and also with the College of Ocean and Earth Sciences, Xiamen University, Xiamen, Fujian 361005, China (e-mail: ftong@xmu.edu.cn; zhuzhengliang@stu.xmu.edu.cn).

Digital Object Identifier 10.1109/TVT.2022.3181801

those in shallow water or in the upper layer of deep sea. Thus, the above CS algorithms derived under the assumption of static sparse or dynamic sparse generally do not take this type of hybrid sparsity into account [24].

As a result, the sparse recovery performance of these state-of-the-art methods significantly decreases at the presence of the hybrid sparsity. To be specific, while improving the estimation of static sparse elements, the SOMP algorithm is subject to performance degradation as the time-varying sparse elements tend to be ignored [17], [18]. Meanwhile, when applying KF-CS for time-varying sparsity, those static sparse components will cause mismatch to the dynamic assumption.

By formulating the sparse UWA channels as sparse set including static and time-varying elements, a static-dynamic discriminative compressed sensing (SDD-CS) algorithm is proposed to exploit the hybrid sparsity of UWA channel [24]. However, as the SDD-CS algorithm separated the time-varying components and then applied sparse estimation under the KF-CS framework, the presence of rapidly time-varying multipath arrivals that cannot be formulated by Kalman dynamic model would cause significant performance degradation. This is because, for the conventional KF-CS type algorithms, the sparse UWA channel is assumed to change slowly with time [23].

Previously several strategies have been investigated for estimating rapidly time-varying underwater acoustic channels. The adaptive subspace-tracking reduced-rank amplitude estimation using the RLS method (ASRAE-RLS) and the adaptive subspace-tracking reduced-rank model-based amplitude estimation method (ASRMAE) [25] have been proposed for improving the rapidly time-varying UWA channel estimation, respectively, however, the classic adaptive filter based algorithms can not efficiently exploit the sparsity structure of the UWA channel. By predicting the cluster-based channel parameters and reconstructing a virtual current received signal, the temporal multiple sparse Bayesian learning (TMSBL) method [26] has been applied to estimate rapidly time-varying channel in UWA OFDM communications. However, the practical UWA channel is not always in cluster structure. In addition, in [27] the Delay-Doppler spread function based algorithm is adopted to estimate rapidly time varying channel in Delay-Doppler domain, which unfortunately needs huge computational complexity to resolve the two-dimensional solution over a large doubly spread UWA channel.

Motivated by previous efforts for exploiting static and time-varying sparsity, the core contribution of this paper is that, by similarly decomposing the sparse components into static elements and dynamic ones, sparse reconstruction with gradient descent variable measurement length was proposed for estimating rapidly time-varying components instead of KF-CS. Thus, the proposed algorithm can equivalently convert the rapidly time-varying channel estimation problem into the multiple short-time stationary channels estimation problem.

Recently, various algorithms have been proposed to improve the quality of joint sparse recovery, such as rank-aware-order recursive matching pursuit (RA-ORMP) [28], compressive MUSIC (CS-MUSIC) [29], subspace-augmented MUSIC (SA-MUSIC) [30], and signal space matching pursuit (SSMP) [31]. However, compared with SOMP algorithm, [31] revealed that the above algorithms achieved similar recovery performance in channels with a high degree of sparsity, at the expense of extra computational burdens.

Hence, similar to the previous SDD-CS strategy, firstly the SOMP is applied to separate and estimate the relatively static sparse elements, which provides the static components estimation by joint sparsity recovery. Next, the residual error of the SOMP is used to reconstruct the time-varying component by the OMP. Considering that, for OMP processing, a shorter observation length leads to enhanced capability of time variation estimation, the novelty of this paper is to adaptively tune the observation length of measurement-wise OMP along the descent gradient to adapt to different level of time variation. Finally, the results of static and time-varying component are summed up to form the whole hybrid sparse solution. Thus, by applying the SOMP and observation length adjustable measurement-wise OMP on the static and the remained dynamic sparse elements respectively, the proposed algorithm, referred as sequential adaptive observation length orthogonal matching pursuit (SAOLOMP) algorithm, is derived for efficient exploitation of rapidly time-varying sparsity contained in UWA channel.

Note that in the case when the static component estimation is inaccurate, such as when the static multipath experiences drastic amplitude variation, the resulting estimation error becomes a part of residual error. By applying viable observation length OMP on the residual error, "static" multipath component that caused this type of inaccurate estimation is actually equivalent to rapidly time-varying multipath.

Numerical simulation as well as the field test in shallow and deep sea were carried out to verify the effectiveness of the proposed algorithm in exploring rapidly time-varying sparsity to improve UWA communication performance. Note that, while the Least Square QR-factorization (LSQR) [32] and the OMP algorithm provided comparison baseline in terms of typical non-sparse and greedy sparse algorithm, SDD-CS, SOMP, and SL0 algorithm [12] were selected as comparison algorithm as the representative of static-dynamic discriminative CS, distributed CS, and norm type CS strategies, respectively.

The rest content of this paper is as follows. Section II describes the system model of UWA communication and the classic OMP and SOMP algorithms. Section III analyzes the impact of rapidly time-varying UWA channel, and introduces the proposed SAOLOMP algorithm and the brief discussion. Section IV presents the numerical simulations. Section V analyzes the field experiment results from both shallow and deep sea. Finally, we make the conclusion in Section VI.

Notation: Bold capital letters denote matrices. The set operations $\cup$ and $\setminus$ denote the union operation and difference operation, respectively. The operation $\mathbf{A} \sqcup \mathbf{B}$ denotes the concatenation between vectors $\mathbf{A}$ and $\mathbf{B}$. ϕ denotes the empty set. $||\mathbf{x}||$ represents the l_2 norm (Euclidean norm) of the vector $\mathbf{x}$. $||\mathbf{x}||_1$ refers to the l_1 norm, which is the sum of the absolute value of each vector element. $\mathbf{A}^\dagger$ represents the matrix pseudo inverse. The set $[i, j]$ denotes the set $[i, i+1, \ldots, j]$. T^c denotes the complement of T which is in $[i, j]$, i.e. $T^c = [i, j] \setminus T$. $\mathbf{A}_{[i,j],[p,k]}$

denotes a sub-matrix obtained from i-th to j-th rows and p-th to k-th columns of $\mathbf{A}$.

II. System Model

A. System Model of UWA Communication

The UWA communication signal can be expressed by [14]

$$y(i) = \sum_{j=0}^{N-1} s(i-j)x(j) + w(i), \quad i = 0, \ldots, M-1, \tag{1}$$

where s, y, w, x are the discrete transmitted signal, recorded signal, additive noise, and UWA channel impulse response (CIR), respectively. M and N are the length of y and x, respectively. To be specific, M is the observation length for the channel estimation. It is an implicit assumption that the UWA channel keeps stationary during the observation period [33].

(1) can be written in matrix format as

$$\mathbf{y} = \mathbf{A}\mathbf{x} + \mathbf{w}, \tag{2}$$

where $\mathbf{y}$, $\mathbf{x}$, $\mathbf{w}$ are the recorded UWA signal, UWA CIR, and additive noise in the vector form, respectively. The measurement matrix $\mathbf{A} \in \mathbb{C}^{M\times N}$ can be obtained from the transmitted signal as following,

$$\mathbf{A} = \begin{pmatrix} s(0) & \cdots & s(-N+1) \\ s(1) & \cdots & s(-N+2) \\ \vdots & \ddots & \vdots \\ s(M-1) & \cdots & s(M-N) \end{pmatrix}. \tag{3}$$

Evidently, estimation of UWA channel $\mathbf{x}$ in (2) can be converted to a compressed sensing problem, and search for the sparse solution of $\mathbf{x}$, where the sparsity factor κ is the number of non-zero elements in $\mathbf{x}$.

B. OMP and SOMP Algorithm

Iterative greedy algorithms have been developed to recover the sparse channel $\mathbf{x}$ from the recorded signal $\mathbf{y}$, among which the OMP algorithm has been proven to successfully recover the acquired signal from incoherent measurements with high probability [34]. The optimization problem of the sparse recovery can be described by [14]

$$\arg\min ||\mathbf{x}||_1 \quad \text{s.t.} \quad ||\mathbf{y} - \mathbf{A}\mathbf{x}||_2^2 \le \varepsilon, \tag{4}$$

where ε is the noise factor. The OMP algorithm iteratively selects the vectors from the matrix $\mathbf{A} \in \mathbb{C}^{M\times N}$ that contain most of the energy of the vector $\mathbf{y}$, M is the observation length for the channel estimation. The sparse solution $\mathbf{x}$ at each iteration is made based on inner products between the columns of $\mathbf{A}$ and a residual. The residual reflects the component of $\mathbf{y}$ that is orthogonal to the previously selected columns.

This algorithm is popular because it can be easily implemented. Besides, there will be no columns selected twice since the residual is always orthogonal to the selected columns, so that computational complexity of algorithm can be reduced [35].

For sparse UWA channel with common support, distributed compressed sensing is capable to further improve the performance of sparse recovery by exploiting the joint sparsity [15], [16]. According to the Joint Sparsity Models 2 (JSM2) of distributed compressed sensing theory theory [16], when the sparse channel measured in adjacent times has similar non-zero elements but different magnitudes, among multiple continuous measurement window the sparse channels can be modeled as sparse solutions with common support, the common support is the location of the static sparse elements. It means that sparse set among adjacent measurements can be reconstructed jointly by employing distributed compressed sensing method.

Under the JSM2 model, the UWA channel $\mathbf{x}_t$ of the t-th measurement can be written as [15]:

$$\mathbf{x}_t = \mathbf{\Psi}_t\mathbf{\Omega} + \mathbf{d}_t, \quad t \in (1, 2, \ldots, D), \tag{5}$$

where $\mathbf{\Omega}$ and $\mathbf{d}_t$ are the common supports and different multipath arrivals in D measurements, respectively. $\mathbf{\Psi}_t$ is the magnitudes of the common supports, D is the number of measurements used for joint sparse recovery. Therefore, the UWA channel of D continuous measurements is composed of two forms of elements, namely, elements with the common supports $\mathbf{\Omega}$, but different magnitudes $\mathbf{\Psi}_t$, and those with different multipath arrivals $\mathbf{d}_t$. Based on the JSM2 framework, estimation of sparse channel can be transformed into the following problem

$$\arg\min \sum_{t=1}^{D} (||\mathbf{x}_t||_1) \quad \text{s.t.} \quad ||\mathbf{Y} - \mathbf{A}\mathbf{X}||_2^2 \le \varepsilon, \tag{6}$$

where

$$\mathbf{Y} = [\mathbf{y}_1, \ldots, \mathbf{y}_D], \mathbf{Y} \in \mathbb{C}^{MD\times 1}, \tag{7a}$$

$$\mathbf{X} = [\mathbf{x}_1, \ldots, \mathbf{x}_D], \mathbf{X} \in \mathbb{C}^{ND\times 1}, \tag{7b}$$

ε is the noise factor, $\mathbf{y}_t$ is the recorded signal of the t-th measurement. The measurement matrix $\mathbf{A}$ can be described by

$$\mathbf{A} = \begin{pmatrix} \mathbf{A}_1 & 0 & \cdots & 0 \\ 0 & \mathbf{A}_2 & \cdots & 0 \\ \vdots & \vdots & \ddots & \vdots \\ 0 & 0 & \cdots & \mathbf{A}_D \end{pmatrix}, \quad \mathbf{A} \in \mathbb{C}^{MD\times ND}, \tag{8}$$

where $\mathbf{A}_t$ is the measurement matrix of the t-th measurement. The constraint condition for (6) is that, all the UWA channel includes several non-zero elements with common supports, while the sparsity of each UWA channel may be different. Especially, as $D = 1$, the SOMP algorithm becomes the classic OMP algorithm.

III. Derivation of the Proposed Algorithm

A. The Observation Length of Rapidly Time-Varying UWA Channel

As shown in (1), for classic channel estimation equation, there is an implicit assumption that the UWA channel is stationary during the observation period. In other words, the observation length M for channel estimation should be smaller than the coherence time of UWA channel. Otherwise, for rapidly time-varying UWA

channel in which observation length M may be larger than the channel coherence time, inherent channel estimation error would be unavoidably generated to degrade the performance of channel estimator. Therefore, tuning the observation length with respect to channel time-varying degree is vital for estimating time-varying channel.

The received signal in (2) can be rewritten as

$$\mathbf{y} = \mathbf{A}_{[1,M],[1,N]}\tilde{\mathbf{x}} + \mathbf{w}, \tag{9}$$

where $\tilde{\mathbf{x}}$ is the estimated channel at time period $[1, M]$. The UWA channel that experiences rapidly time-varying at period $[1, M]$ can be approximately decomposed into short-time stationary channels in p subperiods. Let subperiods

$$M = Q_1 + Q_2 + \cdots + Q_p, \tag{10}$$

where $Q_j, j \in (1, 2, \ldots, p)$, are the duration of each stationary subperiod. Therefore, the (2) can be described precisely by

$$\begin{aligned}\mathbf{y} &= \bigsqcup_{k=1}^{p} \mathbf{y}_{\left[\left(\sum_{j=1}^{k} Q_{j-1}+1\right),\left(\sum_{j=1}^{k} Q_j\right)\right],1} \\ &= \bigsqcup_{k=1}^{p} \mathbf{A}_{\left[\left(\sum_{j=1}^{k} Q_{j-1}+1\right),\left(\sum_{j=1}^{k} Q_j\right)\right],[1,N]} \tilde{\mathbf{x}}_k + \mathbf{w},\end{aligned} \tag{11}$$

where $\sqcup$ is the concatenation operation between vectors, $Q_0 = 0$, $\tilde{\mathbf{x}}_k \in \mathbb{C}^{N\times 1}$ is the estimated channel for time period $[(\sum_{j=1}^{k} Q_{j-1} + 1), (\sum_{j=1}^{k} Q_j)]$. To formulate rapidly time-varying UWA channel with multiple short-time stationary channels, the objective function of searching the optimal duration $Q_j, j \in (1, 2, \ldots, p)$, to minimize residual error can be expressed by

$$\begin{aligned}&(\hat{Q}_1, \hat{Q}_2, \ldots, \hat{Q}_p) \\ &= \arg\min ||\mathbf{y} - \bigsqcup_{k=1}^{p} \mathbf{A}_{\left[\left(\sum_{j=1}^{k} Q_{j-1}+1\right),\left(\sum_{j=1}^{k} Q_j\right)\right],[1,N]} \tilde{\mathbf{x}}_k||^2.\end{aligned} \tag{12}$$

The solution for (12) can be derived by minimizing the cost function

$$J = ||\mathbf{y} - \bigsqcup_{k=1}^{p} \mathbf{A}_{\left[\left(\sum_{j=1}^{k} Q_{j-1}+1\right),\left(\sum_{j=1}^{k} Q_j\right)\right],[1,N]} \tilde{\mathbf{x}}_k||^2. \tag{13}$$

Thus, the challenging problem of rapidly time-varying channel estimation is equivalent to measurement-wise estimation of short-time stationary channel, which can be implemented by applying estimation algorithm with observation length Q_j adaptively tuned at the j-th subperiod. However, as addressing the (12) is a highly complicated multiple-dimension optimization problem, in the next subsection a gradient descent tuning algorithm is designed to simplify the tuning process.

B. Sequential Adaptive Observation Length Orthogonal Matching Pursuit (SAOLOMP) Algorithm Derivation

With the purpose to deal with rapidly time-varying channel, after the separation of static and time-varying components, an adaptive adjustment equation is designed to tune the observation length, with which the measurement-wise OMP is applied to estimate dynamic elements. The flow chart of the proposed SAOLOMP algorithm is shown in Fig. 1.

Let $(\xi_t)_s$ and $(\xi_t)_v$ denote the residual error of static and dynamic components estimation of the t-th measurement, respectively. Ω_s denotes the column index of selected atom for the SOMP, note that Ω_s remains unchanged when $t \in (1, 2, \ldots, D)$. $(\Omega_t)_v$ denotes the column index of selected atom for the measurement-wise OMP of t-th measurement.

The SAOLOMP algorithm has the following steps:

Input:

D adjacent measurements of recorded signal $\mathbf{Y} = [\mathbf{y}_1, \mathbf{y}_2, \ldots, \mathbf{y}_D], \mathbf{Y} \in \mathbb{C}^{MD\times 1}, \mathbf{A} \in \mathbb{C}^{MD\times ND}$; the maximum iterations K for static elements; threshold $v_{threshold}$ of residual error.

Initialization:

The SOMP residual error as $(\xi_t)_s = \mathbf{y}_t$, and the column index of atom as $\Omega_s = (\Omega_t)_v = \phi$. Meanwhile, we set the initial OMP residual error $(\xi_t)_v = (\xi_t)_s$, where $t \in (1, 2, \ldots, D)$.

Step 1:

We adopt the SOMP algorithm to estimate the static elements by utilizing the correlation among adjacent measurements. Firstly, selecting atom $\mathbf{A}_t$ from $\mathbf{A}$ to perform inner product with residual error $(\xi_t)_s$, and summing the inner product outputs of D adjacent measurements to determine the location corresponding to the maximum value γ_k. Hence, we have

$$\gamma_k = \underset{j=1,2,\ldots,N}{\arg\max} \sum_{t=1}^{D} |\left\langle (\mathbf{A}_t)_{[1,M],[j]}, (\xi_t)_s \right\rangle|, \tag{14}$$

where subscript k is the iteration number. Then, the time delay γ_k is added to the static components index Ω_s as

$$\Omega_s = \Omega_s \cup \gamma_k. \tag{15}$$

Based on the selected static components index Ω_s, we calculate the static elements $(\tilde{\mathbf{x}}_t)_s$ of each measurement of UWA channel with least squares (LS) method as

$$(\tilde{\mathbf{x}}_t)_s = (\mathbf{A}_t)^{\dagger}_{[1,M],[\Omega_s]}\mathbf{y}_t. \tag{16}$$

Next, we calculate and update the residual error $(\xi_t)_s$ as

$$(\xi_t)_s = \mathbf{y}_t - (\mathbf{A}_t)_{[1,M],[\Omega_s]}(\tilde{\mathbf{x}}_t)_s, \tag{17}$$

where $t \in (1, 2, \ldots, D)$. Iteration stops when the iteration times reaches the defined number K and obtain the static elements $(\tilde{\mathbf{x}}_t)_s$, otherwise the iteration continues.

Step 2:

Similar to the SDD-CS algorithm [24], upon the residual error of the SOMP, the measurement-wise OMP is applied to estimate the remained dynamic elements. We also set the OMP residual error $(\xi_t)_v = (\xi_t)_s, t \in (1, 2, \ldots, D)$. Meanwhile, $(\mathbf{y}_t)_v$ is contributed by dynamic elements of recorded signal $(\mathbf{y}_t)$, $(\mathbf{y}_t)_v$ is set as the SOMP residual error $(\xi_t)_v$, i.e.

$$(\mathbf{y}_t)_v = (\xi_t)_v, t \in (1, 2, \ldots, D). \tag{18}$$

The measurement matrix $\mathbf{A}_t$ can be expressed by

$$\begin{aligned}\mathbf{A}_t &= (\mathbf{A}_t)_{[1,M],[\Omega_s \cup \Omega_s^c]} \\ &= (\mathbf{A}_t)_{[1,M],[\Omega_s]} \sqcup (\mathbf{A}_t)_{[1,M],[\Omega_s^c]}\end{aligned}$$

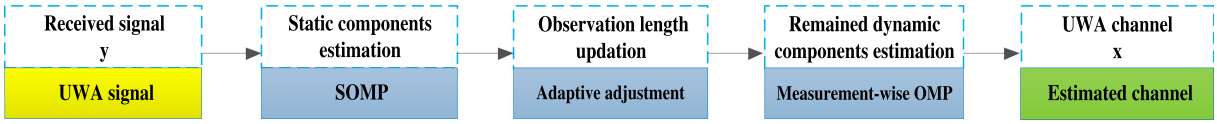

Fig. 1. The flow chart of the proposed SAOLOMP algorithm.

$$= (\mathbf{A}_t)_s \sqcup (\mathbf{A}_t)_v, \tag{19}$$

where Ω_s^c represents the complement of Ω_s, i.e. $\Omega_s^c = [1:N]\backslash\Omega_s$. $(\mathbf{A}_t)_s \in \mathbb{C}^{M\times K}$ and $(\mathbf{A}_t)_v \in \mathbb{C}^{M\times(N-K)}$ denote the term related to dynamic and static elements, respectively. $\sqcup$ is the concatenation operation between matrices, and the concatenation order follows index Ω_s and Ω_s^c.

Meanwhile, as the residual error $(\xi_t)_s$ is mainly contributed by time-varying components of multipath channel, it is used as the cost function of (13), namely,

$$\begin{aligned} J &= ||(\xi_t)_s||^2 \\ &= ||\mathbf{y}_t - (\mathbf{A}_t)_{[1,M],[\Omega_s]}(\tilde{\mathbf{x}}_t)_s||^2 \\ &= \sum_{i=1}^{M} (\mathbf{y}_t(i) - (\mathbf{A}_t)_{[i],[\Omega_s]}(\tilde{\mathbf{x}}_t)_s)^2, \end{aligned} \tag{20}$$

where $t \in (1, 2, \ldots, D)$. While directly addressing the (12) to search optimum observation length is a highly complicated nonlinear optimization problem, inspired by the gradient optimization for filter length [36] or norm strength [37], we expect to derive a gradient descent observation length tuning algorithm by similarly defining the residual error gradient with respect to the observation length as

$$\nabla J_M = \frac{\partial||(\xi_t)_s||^2}{\partial M}, \quad t \in (1, 2, \ldots, D). \tag{21}$$

However, while the magnitude of residual error in (20) indicates the match of the channel time variation and the observation length, directly using the residual error gradient ∇J_M in (21) may lead to negative effect. The reason is that, as revealed in (20), J is equal to the product of M and the mean square of $(\xi_t)_s$, and ∇J_M actually is the mean square of $(\xi_t)_s$. It means that descent gradient with ∇J_M will be only along the direction of discreasing M, thus unsuitable for optimum M search.

Note that transient gradient of residual error with respect to the static sparse element $(\tilde{\mathbf{x}}_t)_s$ can be expressed by

$$\begin{aligned} \nabla J_{(\tilde{\mathbf{x}}_t)_s} &= \frac{\partial||(\xi_t)_s||^2}{\partial(\tilde{\mathbf{x}}_t)_s} \\ &= -2(\xi_t)_s(\mathbf{A}_t)_{[1,M],[\Omega_s]}, \end{aligned} \tag{22}$$

where the size of the measurement matrix $(\mathbf{A}_t)_{[1,M],[\Omega_s]}$ contains the observation length M, i.e., the gradient $\nabla J_{(\tilde{\mathbf{x}}_t)_s}$ implicitly indicates the impact of M on residual error. Meanwhile, to avoid the negative effect of ∇J_M, $\nabla J_{(\tilde{\mathbf{x}}_t)_s}$ can be used for tuning M along the negative direction in the sense that it will approach to minimum point upon the optimum M. Thus, different from the gradient descent derivation in [36] that directly adopted the error gradient with respect to the filter length, the gradient of residual error with respect to the static sparse element $(\tilde{\mathbf{x}}_t)_s$ as defined in (22) is adopted to search the optimum M along the descent direction.

Although herein we cannot give a theoretical optimal derivation, the gradient optimization provides an effective method to solve this observation length optimization problem from the viewpoint of gradient approximation. Thus, a sub-optimal observation length is adaptively tuned to fit the UWA channel with rapidly time-varying multipath as

$$\begin{aligned} (M_t)_v &= \text{ceil}\left(M - \frac{1}{2}\mu||\nabla J_{(\tilde{\mathbf{x}}_t)_s}||\right) \\ &= \text{ceil}(M + \mu||(\xi_t)_s(\mathbf{A}_t)_{[1,M],[\Omega_s]}||), \end{aligned} \tag{23}$$

where μ is the step size, ceil($\mathbf{B}$) represents round the elements of $\mathbf{B}$ to the nearest integers greater than or equal to $\mathbf{B}$, $t \in (1, 2, \ldots, D)$. Therefore, the measurement matrix

$$(\mathbf{A}_t)_v = (\mathbf{A}_t)_{[1,(M_t)_v],[\Omega_s^c]} \tag{24}$$

is the size of $(M_t)_v \times (N-K)$ matrix, the term $(\mathbf{y}_t)_v$ is the size of $(M_t)_v \times 1$ vector, where $t \in (1, 2, \ldots, D)$.

Step 3:

For the dynamic elements estimation, the measurement-wise OMP is proposed to adapt to rapid time variations of UWA channel. Firstly, we select atom $\mathbf{A}_t$ from $(\mathbf{A}_t)_v$ to perform inner product with residual error $(\xi_t)_v$, and determine the location corresponding to the maximum value $(\gamma_t)_k$.

$$(\gamma_t)_k = \underset{j=1,2,\ldots,N-K}{\arg\max} |\left\langle (\mathbf{A}_t)_{[1,(M_t)_v],[j]}, (\xi_t)_v \right\rangle|, \tag{25}$$

where subscript k is the iteration number, and $t \in (1, 2, \ldots, D)$ represents D adjacent measurements. Then, we update the dynamic components index $(\Omega_t)_v$ as

$$(\Omega_t)_v = (\Omega_t)_v \cup (\gamma_t)_k. \tag{26}$$

Based on the index $(\Omega_t)_v$, we calculate the dynamic elements $(\tilde{\mathbf{x}}_t)_v$ of UWA channel with LS method as

$$(\tilde{\mathbf{x}}_t)_v = (\mathbf{A}_t)^{\dagger}_{[1,(M_t)_v],[(\Omega_t)_v]}(\mathbf{y}_t)_v. \tag{27}$$

Next, the residual error $(\xi_t)_v$ is updated as

$$(\xi_t)_v = (\mathbf{y}_t)_v - (\mathbf{A}_t)_{[1,(M_t)_v],[(\Omega_t)_v]}(\tilde{\mathbf{x}}_t)_v, \tag{28}$$

where $t \in (1, 2, \ldots, D)$. Iterations stop when the current residual $(\xi_t)_v$ is smaller than the threshold $v_{threshold}$, thus the dynamic elements $(\tilde{\mathbf{x}}_t)_v$ are obtained.

Step 4:

Finally, the whole sparse solution of the UWA channel is obtained by summing up the static and dynamic elements as

$$\tilde{\mathbf{x}}_t = (\tilde{\mathbf{x}}_t)_s \sqcup (\tilde{\mathbf{x}}_t)_v, t \in (1, 2, \ldots, D), \tag{29}$$

TABLE I
PSEUDO-CODES OF THE PROPOSED ALGORITHM

Given $D, \mathbf{A}, \mathbf{y}, v_{threshold}, K, \mu, M$

Initialize
$(\xi_t)_s = \mathbf{y}_t;\ \Omega_s = (\Omega_t)_v = \phi, t \in (1, 2, ..., D)$
Repeat
  for $k = 1 : K$
    $\gamma_k = \underset{j=1,2,\cdots,N}{\arg\max} \sum_{t=1}^{D} |\left\langle (\mathbf{A}_t)_{[1,M],[j]}, (\xi_t)_s \right\rangle|$
    $\Omega_s = \Omega_s \cup \gamma_k$
    $(\tilde{\mathbf{x}}_t)_s = (\mathbf{A}_t)^{\dagger}_{[1,M],[\Omega_s]} \mathbf{y}_t$
    $(\xi_t)_s = \mathbf{y}_t - (\mathbf{A}_t)_{[1,M],[\Omega_s]} (\tilde{\mathbf{x}}_t)_s, t \in (1, 2, ..., D)$
  endfor
  $(M_t)_v = \text{ceil}(M + \mu||(\xi_t)_s(\mathbf{A}_t)_{[1,M],[\Omega_s]})||, t \in (1, 2, ..., D)$
  Set $k = 1, (\xi_t)_v = (\xi_t)_s, (\mathbf{y}_t)_v = (\xi_t)_s$
  while $(\xi_t)_v > v_{threshold}$
    for $t = 1 : D$
      $(\gamma_t)_k = \underset{j=1,2,\cdots,N-K}{\arg\max} |\left\langle (\mathbf{A}_t)_{[1,(M_t)_v],[j]}, (\xi_t)_v \right\rangle|$
      $(\Omega_t)_v = (\Omega_t)_v \cup (\gamma_t)_k$
      $(\tilde{\mathbf{x}}_t)_v = (\mathbf{A}_t)^{\dagger}_{[1,(M_t)_v],[(\Omega_t)_v]} (\mathbf{y}_t)_v$
      $(\xi_t)_v = (\mathbf{y}_t)_v - (\mathbf{A}_t)_{[1,(M_t)_v],[(\Omega_t)_v]} (\tilde{\mathbf{x}}_t)_v$
    endfor
    $k = k + 1$
  endwhile
Output $\tilde{\mathbf{x}}_t = (\tilde{\mathbf{x}}_t)_s \sqcup (\tilde{\mathbf{x}}_t)_v, t \in (1, 2, ..., D)$

TABLE II
COMPUTATIONAL COMPLEXITY

Algorithms	Computational complexity
LSQR	$\mathcal{O}((3M + 5N)I))$
OMP	$\mathcal{O}(\kappa MN)$
SOMP	$\mathcal{O}(\kappa MN)$
SL0	$\mathcal{O}(M^2 N)$
SDD-CS	$\mathcal{O}(\kappa MN + KMN_s + N_v^3)$
SAOLOMP	$\mathcal{O}(KMN + (\kappa - K)M_v(N - K))$

where $\sqcup$ is the concatenation operation between vectors, and the concatenation order follows index Ω_s and $(\Omega_t)_v$. The iteration procedures above indicate that, the proposed SAOLOMP method is capable of not only making fully use of the hybrid sparse feature of the UWA channel by separating static and dynamic sparse components, but also exploiting the rapidly time-varying sparsity by adaptive observation length adjustment.

The proposed SAOLOMP algorithm is described using MATLAB like pseudo-codes as Table I.

C. Brief Discussion

1) Parameter Choice: Since the proposed SAOLOMP algorithm contains discriminative estimation, the parameters K and $v_{threshold}$ have the impact on the different dynamic sparsity ratio. Larger K would lead to more contribution for static components, which is good for the UWA channel with slowly time-varying sparsity, and vice versa. On the other hand, larger $v_{threshold}$ would result to more details for dynamic components. Thus, in practical terms, suitable K and $v_{threshold}$ value should be taken into account.

2) Computational Complexity Analysis: Table II shows the approximate computational complexity of the proposed SAOLOMP algorithm, as well as the LSQR, OMP, SOMP, SL0, and SDD-CS algorithms. The computational complexity represents all operations of the algorithms. Notation: I denotes the iteration times for LSQR algorithm, M and N are the length of observation time and CIR, respectively. Also, N_s and N_v are the length of static multipath and dynamic multipath, respectively, M_v is the observation length for the dynamic components estimation. κ denotes the sparsity factors of UWA channel, K is the iteration times to obtain the static elements for the SAOLOMP algorithm.

The computational complexity for the SAOLOMP algorithm is $\mathcal{O}(KMN + (\kappa - K)M_v(N - K))$ which mainly comes from the static components and dynamic components estimation. Specifically, while the static components are obtained by the SOMP algorithm in K times iteration associated with the computational complexity $\mathcal{O}(KMN)$, the dynamic components correspond to a complexity of $\mathcal{O}((\kappa - K)M_v(N - K))$, which are caused by the measurement-wise OMP algorithm in $(\kappa - K)$ times iteration with observation length M_v and remaining CIR length $(N - K)$. Compared with the OMP and the SOMP algorithms, the computational complexity for the SAOLOMP algorithm is slightly reduced, since the observation length M_v is shorter than M to fit the UWA channel with different time-varying sparsity. Moreover, the SDD-CS method needs to decompose hybrid multipath arrivals into static and time-varying components, which correspond to additional computation.

3) Recovery Guarantee: In order to analyze the performance of the compressed sensing algorithm, the restricted isometry property (RIP) framework has been widely applied [38]–[40]. Suppose that there exists a constant $\delta \in (0, 1)$ such that

$$(1 - \delta)||\mathbf{x}||_2^2 \leq ||\mathbf{A}\mathbf{x}||_2^2 \leq (1 + \delta)||\mathbf{x}||_2^2, \tag{30}$$

for all κ-sparse vector $\mathbf{x}$. Then, the matrix $\mathbf{A}$ is said to satisfy the RIP. Specifically, the smallest δ satisfying (30) is called the RIP constant of $\mathbf{A}$ and is denoted by δ_κ.

Over the years, various RIP-based recovery guarantees of OMP have been proposed [38]–[43]. [40] presented an optimal RIP condition for the success of the OMP algorithm, when the l_2-normalized sampling matrix is employed. Furthermore, [39] showed the nearly optimal restricted isometry condition for rank aware order recursive matching pursuit (RA-ORMP) to accurately recover the joint sparse vectors if a sampling matrix has unit l_2-norm, and also provided the performance guarantee of RA-ORMP in the more realistic scenarios of general sampling matrices. Note that, by tuning the observation length, the proposed SAOLOMP algorithm is equivalent to converting the problem of the time-varying sparse recovery into multiple short-time sparse recovery, which enables classic RIP-based performance analysis. In the future we will investigate the sufficient condition for SAOLOMP algorithm from the perspective of adjustable observation length to ensure the exact support recovery.

IV. Numerical Simulation

In this section, based on the bell-hop [44] toolkit, numerical simulation is conducted to verify the effectiveness of the SAOLOMP algorithm under the artificial UWA channel with slowly and rapidly time-varying sparsity. The original UWA channel is firstly created by the bell-hop toolkit, from which the paths caused by the sea surface artificially imposed with slow time variations and rapid ones, respectively. In particular, to generate the slowly and rapidly time-varying sparsity, the random variation follows normal distribution is imposed on the delay of surface path with a variance of 0.1 and 1, respectively. Meanwhile, the magnitude of sea surface is imposed with different amplitudes of sinusoidal variations. Since the direct path and bottom path are relatively stable, without loss of generality, we assume that the delay of direct path and bottom path remain unchanged, and the magnitude is imposed with different amplitudes of sinusoidal variations to generate some degrees of variation, which is often affected by the ocean environment.

The distance and depth of the simulation channel is set to 500 meters and 10 meters respectively with the transmitter and receiver located at 8 meters and 10 meters below the sea surface, respectively. The length of CIR is $N = 190$ with equivalent sampling rate 4000 Hz. The observation length is $M = 100$, and the sparsity factor, namely the non-zero element, of the simulated CIR is $\kappa = 6$. The measurement matrix $\mathbf{A}$ is formed by the quadrature phase shift keying (QPSK) symbols.

The CIR of the simulated UWA channel, of which the 5-th and 6-th path imposed with artificial time variations to simulate surface dynamics, is shown in Fig. 2. It can be noticed from Fig. 2 that compared with Fig. 2(a), the simulated channel in Fig. 2(b) presents obviously more rapid time-varying sparsity.

In the simulation test, the parameters of each method are adjusted to the optimal recovery SNR output (ρ_{CR}) for performance evaluation, where

$$\rho_{CR} = 10\log_{10}||\mathbf{h}||_2^2/||\mathbf{h} - \tilde{\mathbf{h}}||_2^2, \tag{31}$$

and $\tilde{\mathbf{h}}$ is the estimated impulse response. The received SNR $\rho_{\mathbf{y}} = 30$ dB, and it is assumed that the sparsity factors κ is known for all the methods beforehand. For the SAOLOMP, SDD-CS, and SOMP algorithm, the data block D is 6, the step size is $\mu = 0.5$, the maximum iterations $K = 4$, and the threshold $v_{threshold}$ is 5e-1. The error tolerance for the LSQR algorithm is 1e-6. For the SL0 method, the step size of iteration is set to 0.6. The sparsity factor κ is set to 6 for the OMP and SOMP algorithms.

The correlation coefficient ρ [45] provides a measure of time-varying degree of channel. Shown in Fig. 3(a) is the correlation coefficients of channels under different time-varying characteristic, for the UWA channel with slowly time-varying sparsity, the correlation coefficient ρ is all above 0.91. On the other hand, for the UWA channel with rapidly time-varying sparsity, the correlation coefficient ρ shows a significantly decline trend along 0.8. Fig. 3(b) presents the observation length M_v for the dynamic multipath channel estimation of the SAOLOMP algorithm under the UWA channel with slowly and rapidly time-varying sparsity, respectively. For the channel with slowly time-varying sparsity,

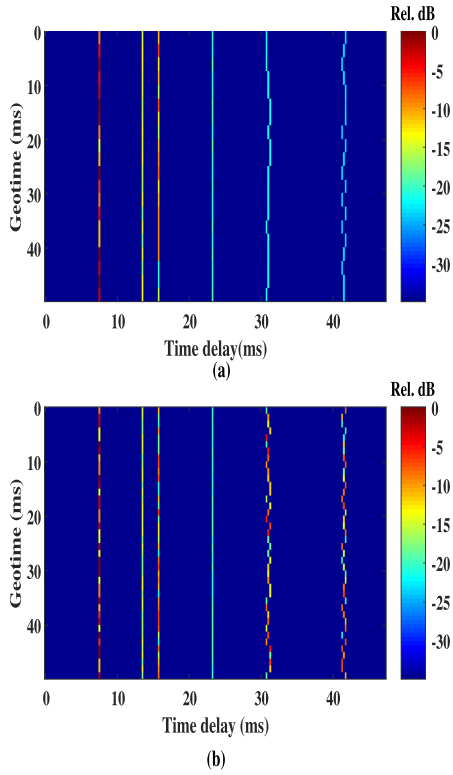

Fig. 2. The simulated UWA channel with slowly and rapidly time-varying sparsity. (a) Channel with slowly time-varying sparsity. (b) Channel with rapidly time-varying sparsity.

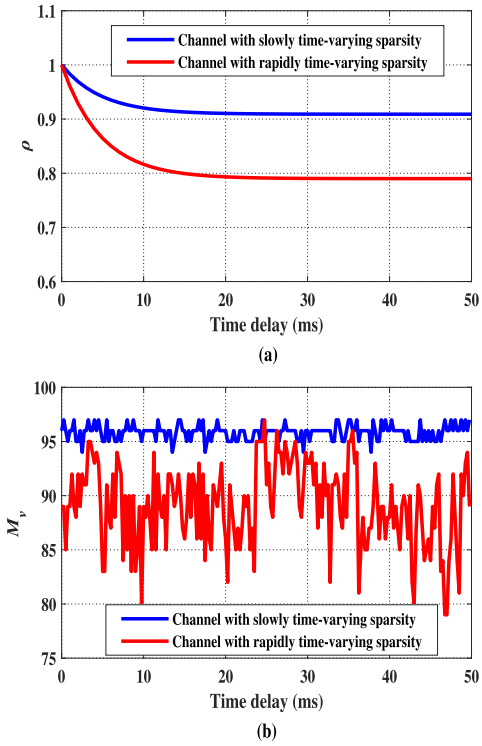

Fig. 3. The correlation coefficient ρ and the observation length M_v under the channel with slowly and rapidly time-varying sparsity. (a) Correlation coefficient. (b) Observation length.

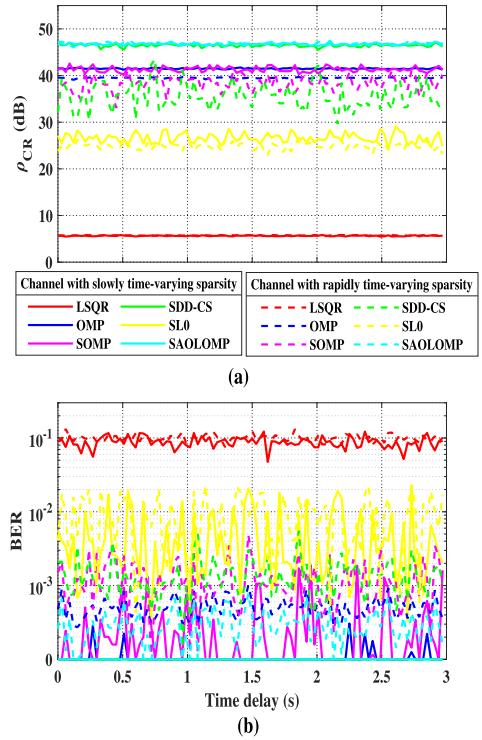

Fig. 4. The outputs of different algorithms under the UWA channel with slowly and rapidly time-varying sparsity. (a) ρ_{CR}. (b) BER.

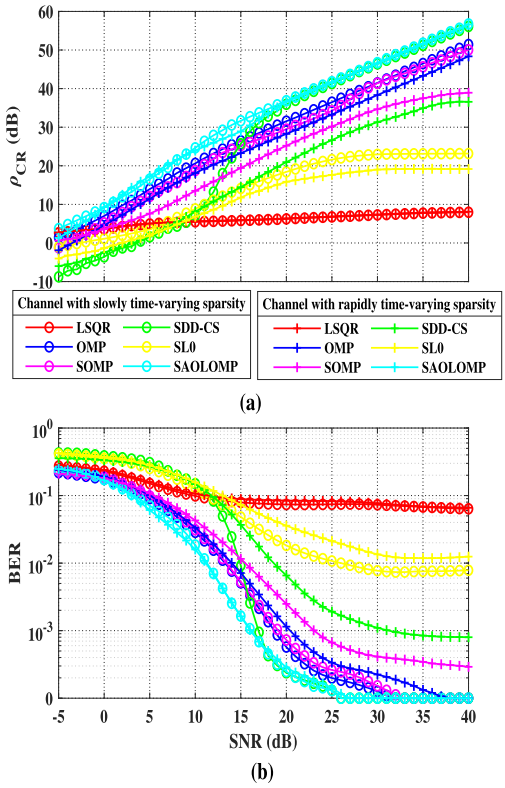

Fig. 5. The outputs of different algorithms with different SNR under the UWA channel with slowly and rapidly time-varying. (a) ρ_{CR}. (b) BER.

the M_v value remains comparatively constant around an averaging length of 96. As the proposed SAOLOMP algorithm enables the tuning capability of M_v according to the gradient of the residual error of the SOMP, the observation length M_v exhibits a much more dynamic trend to adapt to rapidly time-varying sparsity, around an averaging length of 88.

In the numerical simulation, in order to evaluate the communication performance, the linear minimum mean-square error (MMSE) equalizer is adopted to recover the received symbol [46]. The channel recovery SNR (ρ_{CR}) and bit error rate (BER) results obtained by different algorithms are shown in Fig. 4(a) and (b), respectively. One may observe from Fig. 4 that the proposed algorithm achieves the best accuracy among all the algorithms. Meanwhile, it is also evident that, under different time-varying sparsity pattern, the ρ_{CR} and BER output of the SAOLOMP remains stable and robust, while that of the SOMP algorithm is subject to significant performance degradation with rapidly time-varying sparsity. Specifically, because dynamic compressed sensing is designed for recovering the UWA channel with slowly time-varying sparsity, the channel with rapidly time-varying sparsity will cause the model mismatch and significant performance degradation for SDD-CS method. The simulation results demonstrate that the proposed SAOLOMP can adaptively tune the observation length to fit the UWA channel with different time-varying sparsity and is robust to work at the rapidly time-varying sparsity scenario.

The ρ_{CR} and BER outputs of different algorithms with SNR from -5 to 40 dB under the UWA channel with slowly and rapidly time-varying is shown in Fig. 5. As presented in Fig. 5, the main trend of these algorithms is that under different time-varying sparsity pattern, affected by the noise, the ρ_{CR} increases and BER decreases with the SNR from -5 to 40 dB. The proposed SAOLOMP algorithm achieves the highest output SNR ρ_{CR} and the lowest BER among all the other reference algorithms. Specifically, one may also notice that the SDD-CS estimator corresponds to significant performance degradation, as the existence of noise significantly deteriorates the time-varying components tracking, even at the channel with slowly time-varying sparsity.

V. Field Experiment

A. Shallow Sea Experiment

The shallow sea experiment was carried out in the shallow water area at Wuyuan Bay, Xiamen, China, as shown in Fig. 6. The average depth of the experimental site is 7 meters, and the distance between the receiver and the transmitter is about 1000 meters. The signal was transmitted by a transducer suspended at a depth of 4 meters below the sea surface. A four-element receiving array was mounted at the rear of a ship, covering from 1.5 meters to 6 meters below the sea surface with an element spacing of 1.5 meters. The bandwidth of transducer is 13-18 kHz.

The modulation mode is QPSK with a data rate of 8 kbps and a carrier frequency of 16 kHz. The length of CIR is $N = 190$ with equivalent sampling rate 8000 Hz for the baseband signal and the observation length is $M = 150$. As in the simulation

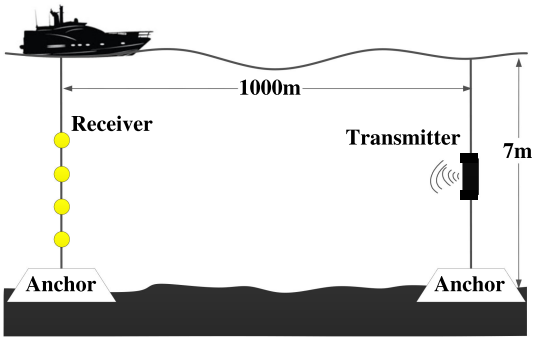

Fig. 6. Setup of the shallow sea experiment.

TABLE III
AVERAGE BER AND ρ_{EO} DRIVEN BY DIFFERENT ESTIMATION ALGORITHMS IN THE SHALLOW SEA EXPERIMENT

Algorithms	BER(%)		ρ_{EO}(dB)	
	Slowly	Rapidly	Slowly	Rapidly
LSQR	4.78	6.68	11.30	10.63
OMP	1.32	2.16	13.39	12.69
SL0	1.49	2.61	13.19	12.53
SOMP	1.08	3.23	13.40	12.13
SDD-CS	0.99	4.38	14.01	11.47
SAOLOMP	0.68	1.07	14.26	13.65

experiment, the parameters of each method are adjusted to the optimal BER output for performance evaluation. Especially, for the SAOLOMP algorithm, the data block D is 5, the step size is $\mu = 0.5$, the maximum iterations $K = 4$, and the threshold $v_{threshold}$ is 5e-1. For the SL0 method, the step size of iteration is set to 0.7. The error tolerance for the LSQR algorithm is 1e-6. The sparsity factor κ is set to 15 for the OMP and SOMP algorithms. For the SOMP and the SDD-CS algorithm, the data block D is set to 5 either.

The time-varying channel response of the four different UWA channels are shown in Fig. 7. It can be seen from Fig. 7 that, as the shallow water geometry leads to serious sea surface and bottom interactions for sound propagation, all the four channels exhibit typical hybrid sparse structure comprising of a group of comparatively static multipath arrivals and some rapidly time-varying ones. To be specific, in these four channels, except some obvious rapidly time-varying multipath, the relatively static multipath arrivals are at the time delay of 6.1 ms, 6.6 ms, 6.1 ms and 7.1 ms, 5.9 ms and 6.4 ms, respectively.

Given in Fig. 8(a) is the channel correlation coefficients of the four different UWA channels corresponding to four receiving elements, from which one may observe that four UWA channels exhibit different degree of time-varying, with the channel 1 and channel 4 experiencing most rapid and slow time-varying behavior. Moreover, Fig. 8(b) provides the observation length M_v during processing of the proposed SAOLOMP algorithm for the four different channels. It can be found from Fig. 8(a) and (b) that, while M_v for all the four channels exhibit frequent variations as driven by the gradient of the SOMP residual error, M_v associated with channel 1 and channel 4 corresponds to the bigger and smallest averaging value, respectively.

In the shallow sea experiment, the multi-channel time reversal (TR) receiver with periodical channel estimate updating is adopted for performance evaluation in terms of receiver output [47], which consists of a multi-channel TR processor and a single-channel RLS algorithm driven decision feedback equalization (DFE) to address the residual inter-symbol interference. A second-order phase locked loop is implanted in the DFE to compensate the residual carrier phase offset.

The data packet of the shallow sea test totally contains 25000 symbols, i.e., 50000 bits, of which a 1000-symbol-long preamble precedes the data packet for initialization of the channel estimate and DFE. Periodic 200 training symbols were inserted between 300 symbol data blocks to retrain the receiver. The data packet structure is shown in Fig. 9. The single-channel adaptive DFE followed the combing time reversal is updated with RLS algorithm. The filter length of the RLS updating forward and backward are set to 32 and 16, respectively, with the RLS forgetting factor of 0.998.

Considering that among the four channels the channel 1 and channel 4 have the most rapid and most slow time variations, respectively, two types of 3-channel pattern are formed by combining three channels to drive the multi-channel TR receiver for performance evaluation with respect to different time-varying sparsity. Specifically, the channel 1, 2, 3 are combined as the UWA channel pattern with rapidly time-varying sparsity, while the channel 2, 3, 4 are combined as the UWA channel pattern with slowly time-varying sparsity. Therefore, the performance of multi-channel TR receiver driven by different channel estimation algorithm is compared under different time-varying sparsity pattern.

The Output Signal Noise Ratio (ρ_{EO}) is applied to evaluate the accuracy of the solution of sparse recovery as

$$\rho_{EO} = 10\log_{10}||\mathbf{s}||_2^2/||\mathbf{s} - \tilde{\mathbf{s}}||_2^2, \tag{32}$$

where $\mathbf{s}$ is the transmitted symbol, $\tilde{\mathbf{s}}$ denotes the soft output from the receiver. Therefore, the communication metrics of the TR receiver are used to evaluate the performance of channel estimation algorithm, namely, ρ_{EO}, BER, and constellation.

The average BER and ρ_{EO} associated with different channel estimation algorithms under the channel with slowly and rapidly time-varying sparsity are shown in Fig. 10(a) and (b), respectively. As given in Fig. 10(a) and (b), it is evident that all the algorithms experience performance degradation when the channel type changes from slowly time-varying to rapidly time-varying. Meanwhile, the proposed SAOLOMP algorithm outperforms the LSQR and the other compressed sensing channel estimation algorithms under both two types of channel. Note that, while for channel with slowly time-varying sparsity, the SDD-CS algorithm yields only slightly worse BER and ρ_{EO} performance than the proposed algorithms does, for channel with rapidly time-varying channel, the SDD-CS algorithm exhibits much worse BER and ρ_{EO} performance than the proposed algorithm does. The average BER and ρ_{EO} driven by different channel estimation algorithms are presented in Table III, from which similar trend can be noticed. Specifically, when the channel time-varying pattern changed from slow to rapid, a BER degradation of 1.90%, 0.84%, 1.12%, 2.15%, 3.39% and 0.39%

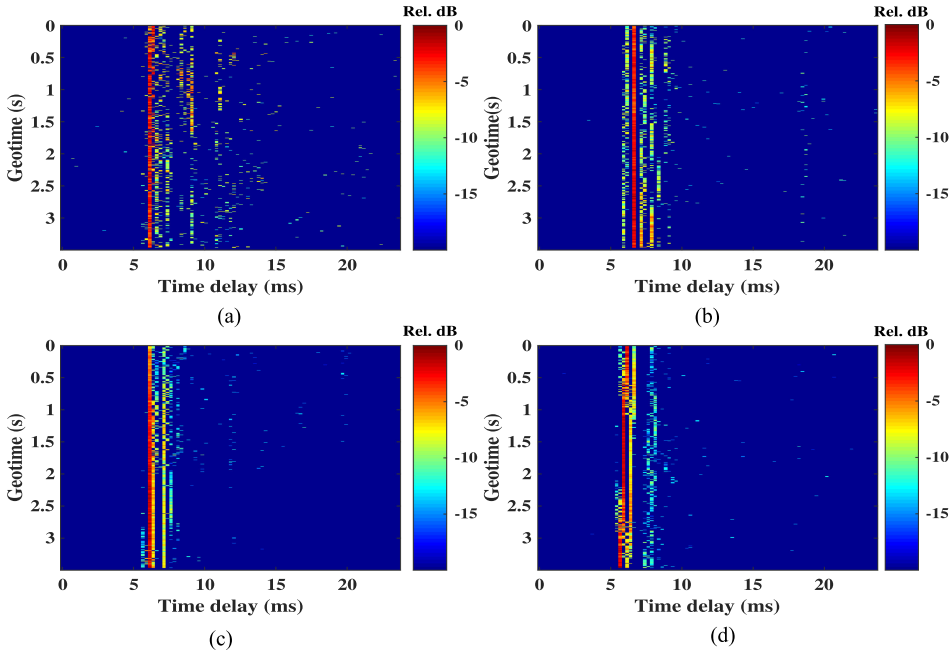

Fig. 7. The CIR of UWA channels obtained by the proposed SAOLOMP method in the shallow sea experiment. (a) Channel 1. (b) Channel 2. (c) Channel 3. (d) Channel 4.

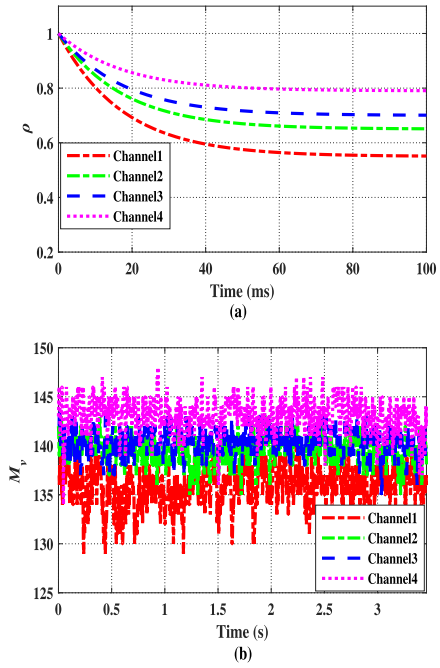

Fig. 8. The channel correlation coefficients ρ and the observation length M_v under four different channels in the shallow sea experiment. (a) Correlation coefficient. (b) Observation length.

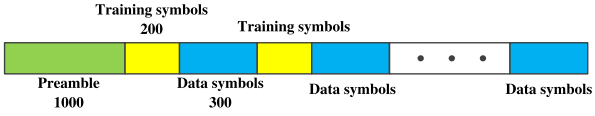

Fig. 9. The formation of the data packet.

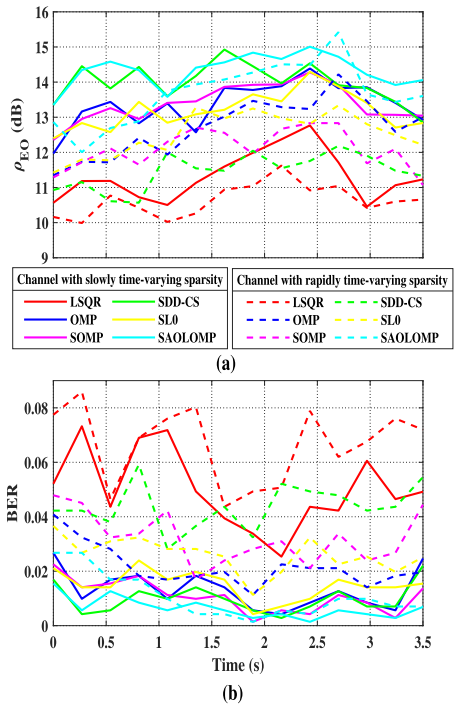

Fig. 10. The outputs driven by different channel estimators under UWA channel with slowly and rapidly time-varying sparsity in the shallow sea experiment. (a) ρ_{EO}. (b) BER.

for the LSQR, OMP, SL0, SOMP, SDD-CS and SAOLOMP algorithm can be observed, respectively.

Moreover, as shown in Table III, under channel with slowly time-varying sparsity, the ρ_{EO} obtained by the receiver driven by the LSQR, OMP, SL0, SOMP, SDD-CS, and SAOLOMP

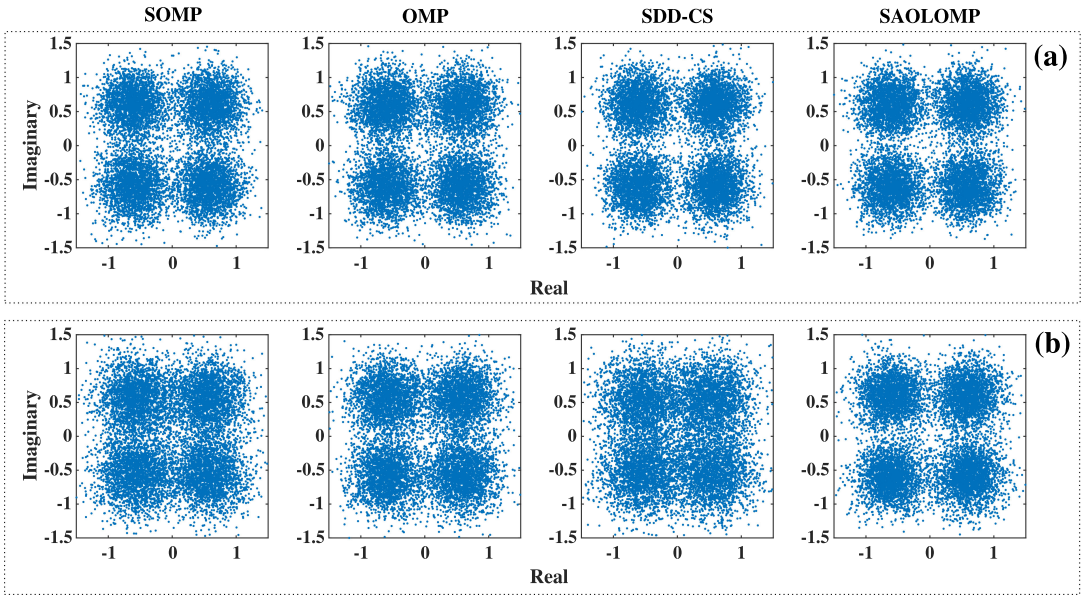

Fig. 11. Constellation outputs driven by different channel estimators in the shallow sea experiment. (a) Under the channel with slowly time-varying sparsity. (b) Under the channel with rapidly time-varying sparsity.

algorithms are 11.30 dB, 13.39 dB, 13.19 dB, 13.40 dB, 14.01 dB, and 14.26 dB, respectively. While for the channel with rapidly time-varying sparsity, the ρ_{EO} of LSQR, OMP, SL0, SOMP, SDD-CS, and SAOLOMP algorithms are 10.63 dB, 12.69 dB, 12.53 dB, 12.13 dB, 11.47 dB, and 13.65 dB, respectively. Similarly, SAOLOMP algorithm corresponds the least performance loss. Note that, while the SDD-CS method achieves the second best BER and ρ_{EO} performance in channel with slowing time-varying sparsity, it experiences the most significant performance degradation in terms of both BER and ρ_{EO}. The reason may be that the Kalman dynamic model used by SDD-CS method to formulate time-varying sparsity fails to track the rapid time variations.

The constellation outputs driven by different channel estimators, namely SOMP, OMP, SDD-CS, SAOLOMP method, under the channel with slowly and rapidly time-varying sparsity are illustrated in Fig. 11, respectively. As shown in Fig. 11, it is clear that for both types of channel pattern, the constellation output of the SAOLOMP algorithm outperforms that of all the other reference algorithms. Meanwhile, the constellation output of SDD-CS exhibits the most obvious performance degradation, when the channel pattern changes from slowly to rapidly time-varying sparsity. Thus, the constellation outputs result is also consistent with the BER and ρ_{EO} results given in Fig. 10 and Table III.

B. Deep Sea Experiment

The deep sea experimental data was collected in south China sea, China. The depth of the experimental area is about 2800 meters, with the transmitter and the receiver located 100 m and 12 m below the water surface, respectively. The distance between the transmitter and the receiver is about 2 kilometers. The transmitter signal is QPSK with a data rate of 8 kbps, and the carrier frequency of 16 kHz. The bandwidth of transducer is 13–18 kHz.

For the channel estimator, the length of CIR is set to $N = 160$ with equivalent sampling rate 8000 Hz for the baseband signal and the observation length is set to $M = 145$. As in the simulation experiment, the parameters of each method are adjusted to the optimal BER output for performance evaluation. Specifically, for the SAOLOMP algorithm, the data block D is 6, the step size is $\mu = 0.5$, the maximum iterations $K = 3$, and the threshold $v_{threshold}$ is 5e-1. For the SL0 method, the step size of iteration is set to 0.75. The error tolerance for the LSQR algorithm is 1e-6. The sparsity factor κ is set to 10 for the OMP and SOMP algorithms. For the SOMP and the SDD-CS algorithm, the data block D is also set to 6.

In the deep sea experiment, a single-channel TR receiver followed by a single-channel DFE is adopted for performance evaluation in terms of the receiver communication metrics, i.e, ρ_{EO}, BER, and constellation. For the RLS algorithm driven DFE, the forward and backward filter length are 32 and 16 respectively, with a forgetting factor of 0.996. While the data packet totally contains 13500 symbols, of which the length of preamble, periodic training symbol and data block is 1000, 175 and 325 symbols, respectively.

The deep sea experimental channel as shown in Fig. 12 belongs to upper channel that contains both direct path and surface-reflection path, corresponding to a steady path at 4 ms delay and an obvious time-varying path at about 7 ms delay, respectively. Fig. 13(a) presents the channel correlation coefficients of the UWA channels to investigate the degree of time-varying. As shown in Figs. 12 and 13(a), the deep sea UWA channel exhibits rapidly time-varying sparsity pattern. Besides, Fig. 13(b) provides the observation length M_v during

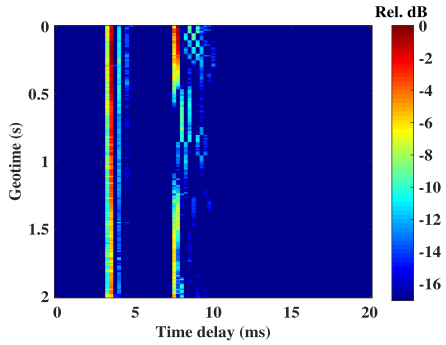

Fig. 12. The CIR of UWA channels obtained by the proposed SAOLOMP method in the deep sea experiment.

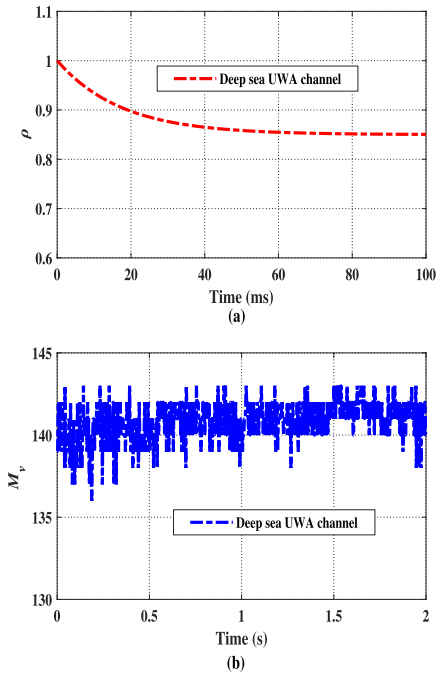

Fig. 13. The channel correlation coefficients ρ and the observation length M_v in the deep sea experiment. (a) Correlation coefficient. (b) Observation length.

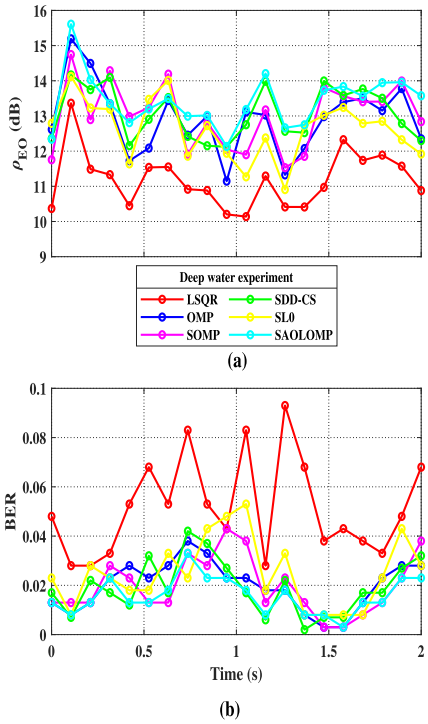

Fig. 14. The outputs driven by different channel estimators in the deep sea experiment. (a) ρ_{EO}. (b) BER.

TABLE IV
AVERAGE BER AND ρ_{EO} DRIVEN BY DIFFERENT ESTIMATION ALGORITHMS IN THE DEEP SEA EXPERIMENT

Algorithms	BER(%)	ρ_{EO}(dB)
LSQR	4.85	11.16
OMP	2.06	12.83
SL0	2.53	12.56
SOMP	1.89	12.94
SDD-CS	1.76	13.02
SAOLOMP	1.60	13.11

processing of the proposed SAOLOMP algorithm. It can be seen from Fig. 13(b) that similar to the curve in Fig. 8, M_v driven by gradient experiences frequent variations to track the channel with time-varying sparsity.

Note that, as revealed in both Figs. 7 and 12, deep sea channel has a stronger stable path than shallow water channel does, thus, although the correlation coefficient curve of the deep sea channel as shown in Fig. 13(a) exhibits less rapidly time-varying than that of the shallow sea channel as shown in Fig. 8(a), time-varying path in deep sea actually experiences similar rapid time-variations as channels in shallow water. It can also be verified by the observation length curves as shown in Figs. 8(b) and 13(b), both of which corresponding to similar average observation length at around 140.

As presented in Fig. 14(a) and Table IV are the ρ_{EO} curve and average ρ_{EO} in the deep sea experiment, respectively. The ρ_{EO} is obtained by the TR-DFE driven by the LSQR, OMP, SL0, SOMP, SDD-CS, and SAOLOMP algorithms, respectively. Especially, while the lowest ρ_{EO} of LSQR is 10.33, the proposed SAOLOMP method generates the highest ρ_{EO} of 13.11, versus 12.83 by OMP, 12.56 by SL0, 12.94 by SOMP and 13.02 by SDD-CS algorithm.

In addition, the BER curve as well as average BER achieved by different channel estimation algorithms in the deep sea experiment are shown in Fig. 14(b) and Table IV, respectively. Among all the six channel estimation methods, the SAOLOMP method realizes the lowest BER output. Due to substantial estimation noise, the LSQR algorithm presents the worst estimation performance. Compared with the proposed SAOLOMP algorithm, the classic compressed sensing channel estimation algorithms, namely, the OMP, SL0, and SOMP algorithms go through markedly performance decrease. Besides, affected by the UWA channel with rapidly time-varying sparsity, SDD-CS method also occurs performance degradation. It is evident that the proposed SAOLOMP algorithm yields the lowest BER 1.6%,

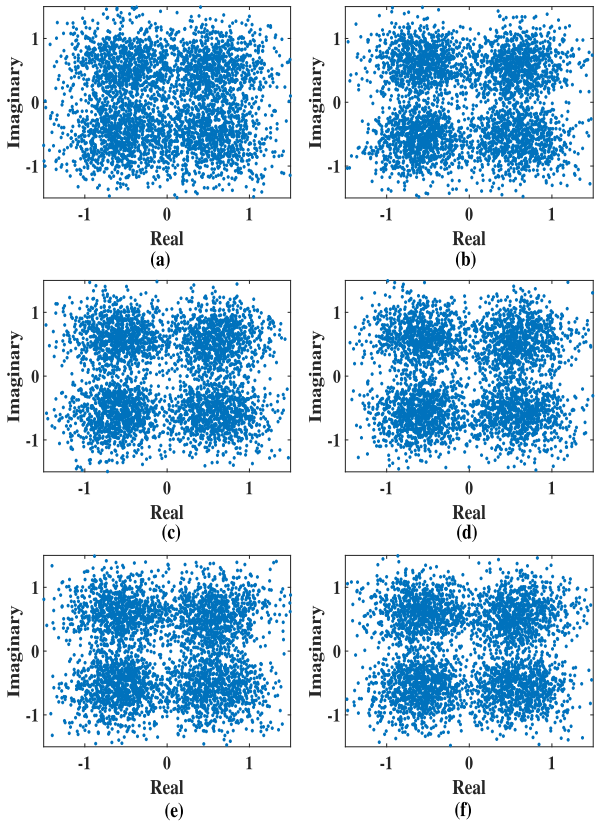

Fig. 15. Constellation outputs driven by different channel estimators in the deep sea experiment. (a) LSQR. (b) OMP. (c) SOMP. (d) SDD-CS. (e) SL0. (f) SAOLOMP.

which corresponding to a reduction of 3.25%, 0.46%, 0.97%, 0.29%, and 0.16% over the LSQR, OMP, SL0, SOMP and SDD-CS algorithm, respectively.

The constellation outputs driven by different channel estimators in the deep sea experiment are illustrated in Fig. 15. It can be found that the LSQR method shows the worse constellation quality, since there is visible estimation noise. The OMP, SOMP, and SL0 estimators can exploit the channel sparsity, or joint sparsity, the estimation results show a great noise abatement effect. However, the UWA channel with rapidly time-varying sparsity will unavoidably bring about considerable performance degradation for the classic compressed sensing channel estimation algorithms. In addition, SDD-CS method yields the second highest constellation quality, while the SDD-CS algorithm is able to exploit hybrid sparsity of UWA channel. Nevertheless, this type of algorithm is designed for the UWA channel with slowly time-varying sparsity, the estimation performance of SDD-CS method would be affected by the rapidly time-varying components. As shown in Fig. 15, it is clear that, the constellation quality of SAOLOMP algorithm is obviously better than the other three sparse algorithms, because the SAOLOMP algorithm is derived to exploit the UWA channel with rapidly time-varying sparsity, and can adaptively tune the observation length to fit the UWA channel with different time-varying sparsity. Therefore, the constellation outputs result in the deep sea experiment is in line with the average BER results in Table IV either.

VI. Conclusion

A sequential adaptive observation length orthogonal matching pursuit (SAOLOMP) algorithm is presented to explore rapidly time-varying sparsity for UWA channels.

The core idea of the proposed algorithm is to firstly adopt the joint sparse recovery SOMP to separate static components. As the residual error of the SOMP processing indicates time variation level of the remained time-varying components, the measurement-wise OMP is performed on the residual error of the SOMP for reconstruction of dynamic component, with the observation length of which adaptively adjusted according to the gradient of residual error. Finally, estimation results of these two components are summed up to obtain the whole hybrid sparse signal, thus enabling efficient identification of rapidly time-varying sparsity via separation of hybrid sparse elements and adaptive observation length adjustment.

Numerical simulations, as well as two typical UWA communication scenarios, i.e., one in shallow sea and one in deep sea, show that, at the presence of rapidly time-varying sparsity, the proposed SAOLOMP algorithm yields better performance, when compared with the classic algorithms.

References

[1] Y. Zhang, Z. Zhang, L. Chen, and X. Wang, "Reinforcement learning-based opportunistic routing protocol for underwater acoustic sensor networks," *IEEE Trans. Veh. Technol.*, vol. 70, no. 3, pp. 2756–2770, Mar. 2021.

[2] M. Stojanovic, "Efficient processing of acoustic signals for high-rate information transmission over sparse underwater channels," *Phys. Commun.*, vol. 1, no. 2, pp. 146–161, 2008.

[3] B. Li, S. Zheng, and F. Tong, "Bit-error rate based doppler estimation for shallow water acoustic OFDM communication," *Ocean Eng.*, vol. 182, pp. 203–210, 2019.

[4] F. Wu, K. Yang, and R. Duan, "Compressed sensing of underwater acoustic signals via structured approximation l_0-norm," *IEEE Trans. Veh. Technol.*, vol. 67, no. 9, pp. 8504–8513, Sep. 2018.

[5] Y. Zhou and R. Diamant, "A parallel decoding approach for mitigating near–far interference in Internet of Underwater Things," *IEEE Internet Things J.*, vol. 7, no. 10, pp. 9747–9759, Oct. 2020.

[6] A. C. Singer, J. K. Nelson, and S. S. Kozat, "Signal processing for underwater acoustic communications," *IEEE Commun. Mag.*, vol. 47, no. 1, pp. 90–96, Jan. 2009.

[7] E. Panayirci, M. T. Altabbaa, and H. V. Poor, "Channel estimation and equalization for alamouti SF-coded OFDM-UWA communications," *IEEE Trans. Veh. Technol.*, vol. 70, no. 2, pp. 1709–1723, Feb. 2021.

[8] Y. Zhang, R. Venkatesan, O. A. Dobre, and C. Li, "Efficient estimation and prediction for sparse time-varying underwater acoustic channels," *IEEE J. Ocean. Eng.*, vol. 45, no. 3, pp. 1112–1125, Jul. 2019.

[9] M. A. Figueiredo, R. D. Nowak, and S. J. Wright, "Gradient projection for sparse reconstruction: Application to compressed sensing and other inverse problems," *IEEE J. Sel. Topics Signal Process.*, vol. 1, no. 4, pp. 586–597, Dec. 2007.

[10] Y. Gu, J. Jin, and S. Mei, "l_0 norm constraint LMS algorithm for sparse system identification," *IEEE Signal Process. Lett.*, vol. 16, no. 9, pp. 774–777, Sep. 2009.

[11] J. Jin, Y. Gu, and S. Mei, "A stochastic gradient approach on compressive sensing signal reconstruction based on adaptive filtering framework," *IEEE J. Sel. Topics Signal Process.*, vol. 4, no. 2, pp. 409–420, Apr. 2010.

[12] H. Mohimani, M. Babaie-Zadeh, and C. Jutten, "A fast approach for overcomplete sparse decomposition based on smoothed l_0 norm," *IEEE Trans. Signal Process.*, vol. 57, no. 1, pp. 289–301, Jan. 2008.

[13] S. G. Mallat and Z. Zhang, "Matching pursuits with time-frequency dictionaries," *IEEE Trans. Signal Process.*, vol. 41, no. 12, pp. 3397–3415, Dec. 1993.

[14] J. A. Tropp and A. C. Gilbert, "Signal recovery from random measurements via orthogonal matching pursuit," *IEEE Trans. Inf. Theory*, vol. 53, no. 12, pp. 4655–4666, Dec. 2007.

[15] J. A. Tropp, A. C. Gilbert, and M. J. Strauss, "Simultaneous sparse approximation via greedy pursuit," in *Proc. IEEE Int. Conf. Acoustics, Speech, Signal Process.*, 2005, vol. 5, pp. 721–724.
[16] S. Corroy and R. Mathar, "Distributed compressed sensing for the MIMO MAC with correlated sources," in *Proc. IEEE Int. Conf. Commun.*, 2012, pp. 2516–2520.
[17] Y. Zhou, F. Tong, and G. Zhang, "Distributed compressed sensing estimation of underwater acoustic OFDM channel," *Appl. Acoust.*, vol. 117, pp. 160–166, 2017.
[18] Y. Zhou, A. Song, F. Tong, and R. Kastner, "Distributed compressed sensing based channel estimation for underwater acoustic multiband transmissions," *J. Acoustical Soc. America*, vol. 143, no. 6, pp. 3985–3996, 2018.
[19] N. Vaswani, "Kalman filtered compressed sensing," in *Proc. 15th IEEE Int. Conf. Image Process.*, 2008, pp. 893–896.
[20] N. Vaswani, "Analyzing least squares and Kalman filtered compressed sensing," in *Proc. IEEE Int. Conf. Acoust. Speech Signal Process.*, 2009, pp. 3013–3016.
[21] J. Zhou, G. Xia, and J. Wang, "OFDM system channel estimation algorithm research based on Kalman filter compressed sensing," *J. Theor. Appl. Inf. Technol.*, vol. 49, no. 1, pp. 119–125, 2013.
[22] W. Jiang, S. Zheng, Y. Zhou, F. Tong, and R. Kastner, "Exploiting time varying sparsity for underwater acoustic communication via dynamic compressed sensing," *J. Acoustical Soc. America*, vol. 143, no. 6, pp. 3997–4007, 2018.
[23] N. Vaswani, "LS-CS-residual (LS-CS): Compressive sensing on least squares residual," *IEEE Trans. Signal Process.*, vol. 58, no. 8, pp. 4108–4120, Aug. 2010.
[24] W. Jiang, F. Tong, S. Zheng, and X. Cao, "Estimation of underwater acoustic channel with hybrid sparsity via static-dynamic discriminative compressed sensing," *IEEE Sensors J.*, vol. 20, no. 23, pp. 14548–14558, Dec. 2020.
[25] S. Huang, T. Yang, and J. Tsao, "Improving channel estimation for rapidly time-varying correlated underwater acoustic channels by tracking the signal subspace," *Ad Hoc Netw.*, vol. 34, pp. 17–30, 2015.
[26] G. Qiao, Q. Song, L. Ma, Z. Sun, and J. Zhang, "Channel prediction based temporal multiple sparse Bayesian learning for channel estimation in fast time-varying underwater acoustic OFDM communications," *Signal Process.*, vol. 175, 2020, Art. no. 107668.
[27] W. Li and J. C. Preisig, "Estimation of rapidly time-varying sparse channels," *IEEE J. Ocean. Eng.*, vol. 32, no. 4, pp. 927–939, Oct. 2007.
[28] M. E. Davies and Y. C. Eldar, "Rank awareness in joint sparse recovery," *IEEE Trans. Inf. Theory*, vol. 58, no. 2, pp. 1135–1146, Feb. 2012.
[29] J. M. Kim, O. K. Lee, and J. C. Ye, "Compressive MUSIC: Revisiting the link between compressive sensing and array signal processing," *IEEE Trans. Inf. Theory*, vol. 58, no. 1, pp. 278–301, Jan. 2012.
[30] K. Lee, Y. Bresler, and M. Junge, "Subspace methods for joint sparse recovery," *IEEE Trans. Inf. Theory*, vol. 58, no. 6, pp. 3613–3641, 2012.
[31] J. Kim, J. Wang, L. T. Nguyen, and B. Shim, "Joint sparse recovery using signal space matching pursuit," *IEEE Trans. Inf. Theory*, vol. 66, no. 8, pp. 5072–5096, Aug. 2020.
[32] M. Jacobsen, P. C. Hansen, and M. A. Saunders, "Subspace preconditioned LSQR for discrete ill-posed problems," *BIT Numer. Math.*, vol. 43, no. 5, pp. 975–989, 2003.
[33] J. A. Tropp, "Greed is good: Algorithmic results for sparse approximation," *IEEE Trans. Inf. Theory*, vol. 50, no. 10, pp. 2231–2242, Oct. 2004.
[34] A. Cohen, W. Dahmen, and R. A. DeVore, *Near Optimal Approximation of Arbitrary Vectors From Highly Incomplete Measurements*. Aachen, Germany: Inst. für Geometrie und Praktische Mathematik, 2007.
[35] M. Elad, *Sparse and Redundant Representations: From Theory to Applications in Signal and Image Processing*. Berlin, Germany: Springer, 2010.
[36] Y. Gu, K. Tang, and H. Cui, "LMS algorithm with gradient descent filter length," *IEEE Signal Process. Lett.*, vol. 11, no. 3, pp. 305–307, Mar. 2004.
[37] F. Wu and F. Tong, "Gradient optimization p-norm-like constraint LMS algorithm for sparse system estimation," *Signal Process.*, vol. 93, no. 4, pp. 967–971, 2013.
[38] S. Kwon, J. Wang, and B. Shim, "Multipath matching pursuit," *IEEE Trans. Inf. Theory*, vol. 60, no. 5, pp. 2986–3001, May 2014.
[39] J. Kim, J. Wang, and B. Shim, "Nearly optimal restricted isometry condition for rank aware order recursive matching pursuit," *IEEE Trans. Signal Process.*, vol. 67, no. 17, pp. 4449–4463, Sep. 2019.
[40] J. Kim, J. Wang, and B. Shim, "Optimal restricted isometry condition of normalized sampling matrices for exact sparse recovery with orthogonal least squares," *IEEE Trans. Signal Process.*, vol. 69, pp. 1521–1536, 2021.
[41] M. A. Davenport and M. B. Wakin, "Analysis of orthogonal matching pursuit using the restricted isometry property," *IEEE Trans. Inf. Theory*, vol. 56, no. 9, pp. 4395–4401, Sep. 2010.
[42] J. Wang and B. Shim, "On the recovery limit of sparse signals using orthogonal matching pursuit," *IEEE Trans. Signal Process.*, vol. 60, no. 9, pp. 4973–4976, Sep. 2012.
[43] Q. Mo and Y. Shen, "A remark on the restricted isometry property in orthogonal matching pursuit," *IEEE Trans. Inf. Theory*, vol. 58, no. 6, pp. 3654–3656, Jun. 2012.
[44] K. Stamatiou, P. Casari, and M. Zorzi, "The throughput of underwater networks: Analysis and validation using a ray tracing simulator," *IEEE Trans. Wireless Commun.*, vol. 12, no. 3, pp. 1108–1117, Mar. 2013.
[45] X. Tu, X. Xu, and A. Song, "Frequency-domain decision feedback equalization for single-carrier transmissions in fast time-varying underwater acoustic channels," *IEEE J. Ocean. Eng.*, vol. 46, no. 2, pp. 704–716, Apr. 2021.
[46] W. Zeng and W. Xu, "Fast estimation of sparse doubly spread acoustic channels," *J. Acoustical Soc. America*, vol. 131, no. 1, pp. 303–317, 2012.
[47] A. Song, A. Abdi, M. Badiey, and P. Hursky, "Experimental demonstration of underwater acoustic communication by vector sensors," *IEEE J. Ocean. Eng.*, vol. 36, no. 3, pp. 454–461, Jul. 2011.

Weihua Jiang (Member, IEEE) received the Ph.D. degree in marine physics with Xiamen University, Xiamen, China, in 2020. From 2018 to 2020, he was a Visiting Student with the Department of Electrical and Computer Engineering, University of Washington, Seattle, WA, USA. He is currently a Postdoctoral Researcher with the Acoustic and Navigation Laboratory, University of Haifa, Haifa, Israel. His research focuses on underwater acoustic communication and network.

Feng Tong (Member, IEEE) received the Ph.D. degree in underwater acoustics from Xiamen University, Xiamen, China, in 2000. From 2000 to 2002, he was a Postdoctoral Fellow with the Department of Radio Engineering, Southeast University, Nanjing, China. From 2003 to 2004, he was a Research Associate with the Department of Manufacturing Engineering and Engineering Management, City University of Hong Kong, Hong Kong. From December 2009 to December 2010, he was a Visiting Scholar with the Department of Computer Science and Engineering, University of California San Diego, La Jolla, CA, USA. He is currently a Professor with the Department of Applied Marine Physics and Engineering, Xiamen University. His research interests include underwater acoustic communication and acoustic signal processing. Dr. Tong is also a Member of the Acoustical Society of China and China Ship Instrument Society. He serves on the Editorial Board for the JOURNAL OF MARINE SCIENCE AND APPLICATION.

Zhengliang Zhu received the B.S. degree from the Changsha University of Science and Technology, Changsha, China, in 2017, and the M.S. degree from Central South University, Changsha, China, in 2020. He is currently working toward the Ph.D degree with the Key Laboratory of Underwater Acoustic Communication and Marine Information Technology of the Ministry of Education, Xiamen University, Xiamen, China. His research interests include UWB radar signal processing and underwater acoustic communication & network.